Solidification of nitrogen-atomized $Al_{86}Ni_6Y_{4.5}Co_2La_{1.5}$ metallic glass

M. Yan
The University of Queensland, School of Mechanical and Mining Engineering, ARC Centre of Excellence for Design in Light Metals, Brisbane, QLD 4072, Australia

J.Q. Wang[a)]
Shenyang National Laboratory for Materials Science, Institute of Metal Research, Chinese Academy of Sciences, Shenyang 110016, China

G.B. Schaffer
The University of Queensland, School of Mechanical and Mining Engineering, ARC Centre of Excellence for Design in Light Metals, Brisbane, QLD 4072, Australia

M. Qian[b)]
The University of Queensland, School of Mechanical and Mining Engineering, ARC Centre of Excellence for Design in Light Metals, Brisbane, QLD 4072, Australia

(Received 16 November 2010; accepted 10 January 2011)

A comprehensive investigation has been made of the solidification of nitrogen-atomized $Al_{86}Ni_6Y_{4.5}Co_2La_{1.5}$, using focused ion beam, transmission electron microscopy, and other analytical means. Face-centered cubic Al_2Y was identified to be the leading crystalline phase rather than crystalline Al. A new orthorhombic-structured phase was identified in partially or fully crystallized powder particles. Apart from oxygen, nitrogen was also found to be associated with the leading crystalline phase Al_2Y in which nitrogen exists as substitutional N^{x-}. These findings facilitate the basis for understanding the unique aspects of the $Al_{86}Ni_6Y_{4.5}Co_2La_{1.5}$ bulk metallic glass, including its powder preparation by gas atomization.

I. INTRODUCTION

Bulk metallic glass (BMG) was first realized in a Pd-based system[1] and subsequently in many other systems such as Fe-based,[2,3] Cu-based,[4,5] Ti-based,[6,7] Mg-based,[8,9] and Zr-based systems.[10–12] The unique microstructural features and properties of BMGs have drawn significant attention from the scientific community.[13,14] Al-based BMGs, however, are only a very recent development; the first Al-based BMG with a composition of $Al_{86}Ni_6Y_{4.5}Co_2La_{1.5}$ (all in at.%) was fabricated in 2009.[15] All other Al-based amorphous alloys known to date are of limited glass forming ability (GFA), being amorphous only to a thickness of a few ten or hundred micrometers.[15,16]

Given the challenges encountered in developing Al-based BMGs, it is necessary to understand the solidification of Al-based BMGs for future development of superior materials. In this regard, powder particles with different diameters offer an attractive start point as they represent a wide range of cooling rates, enabling one to pursue a detailed microstructural study from fully amorphous to fully crystallized states.[17–20] In addition, powder metallurgy (PM) provides a potential solution to the fabrication of Al-based BMGs from amorphous powder,[21,22] particularly when consolidated with the assistance of high pressure such as by spark plasma sintering. It is, therefore, also of necessity to understand the microstructural characteristics of gas-atomized $Al_{86}Ni_6Y_{4.5}Co_2La_{1.5}$ powder particles for BMG fabrication from powder.

Using focused ion beam (FIB), transmission electron microscopy (TEM), and other analytical means, this work presents a comprehensive study of the solidification microstructure of nitrogen-atomized $Al_{86}Ni_6Y_{4.5}Co_2La_{1.5}$ metallic glass powder in a wide size range. The implications of the experimental results are discussed in the context of both BMG development and the PM of metallic glasses.

II. EXPERIMENTAL

$Al_{86}Ni_6Y_{4.5}Co_2La_{1.5}$ powder was prepared by nitrogen atomization through a close-coupled nozzle under a jet of nitrogen at a pressure of 2.7 MPa. The gas velocity at the outlet was estimated to be 204 m/s. The powder particles were collected and kept in a desiccator at room temperature. The powder was sieved into different size ranges (<25, 25–47, 47–75, and >75 μm) for characterization.

Powder particles were analyzed using x-ray diffraction (XRD, Rigaku D/max III, Cu Kα target,

Address all correspondence to these authors.
[a)]e-mail: jqwang@imr.ac.cn
[b)]e-mail: ma.qian@uq.edu.au
DOI: 10.1557/jmr.2011.13

 © Materials Research Society 2011

https://doi.org/10.1557/jmr.2011.13 Published online by Cambridge University Press

operated at 40 kV and 60 mA), scanning electron microscopy (SEM, JEOL 6460 and JEOL 7001, both operated at 15 kV), differential scanning calorimetry (DSC, NETZSCH STA 409 CD, heating and cooling rate at 10 °C/min), x-ray photoelectron spectrometry (XPS, Kratos Axis ULTRA XPS, monochromatic Al x-ray, C1s at 285 eV as a standard), and TEM (Tecnai F20, operated at 200 kV). TEM energy dispersive x-ray (TEM–EDX) spectrometer was used to study the phase composition. TEM samples were prepared from gas-atomized powder particles as follows. First, the atomized powder was mixed with pure Al powder and pressed uniaxially at 300 MPa to form a thin sample disk, where the ductile pure Al powder was used essentially as a binder. Second, the sample disk was mirror-polished. Subsequently, TEM samples were made from sample disks using FIB (XT Nova Nanolab 200, Ga ion source). During FIB processing, care was taken to minimize the effect of the Ga ions on the phase formation in the $Al_{86}Ni_6Y_{4.5}Co_2La_{1.5}$ metallic glass by applying a low beam current. On cross checking the results obtained from TEM and XRD analyses, it was confirmed that the phase formation is not affected by the FIB process.

III. RESULTS AND DISCUSSION

A. The size effect of droplets

Assuming that the heat transfer between a spherical liquid droplet and the gas medium during gas-atomization obeys Newton's law of cooling, the cooling rate of a spherical droplet can be estimated by[23,24]

$$dT/dt = (1/d)[6h \times (T_l - T_c)]/\rho/C \quad , \qquad (1)$$

where T is temperature (K); t is time (s); T_l is the initial temperature of the liquid droplet (T_l = 1200 K with a superheat of 220 K for gas-atomizing);[15] T_c is the temperature of the cooling medium (298 K); ρ is the density of the liquid (3140 kg/m^3);[15] C is the specific heat, taken to be 615.6 J/kg/K based on the experimental data available for a similar Al-based metallic glass;[16] and h is the coefficient of heat transfer, which has been determined for nitrogen[25] and argon.[26] The particle size (d) is inversely proportional to the cooling rate (dT/dt).

Figure 1 plots the calculated cooling rates for the $Al_{86}Ni_6Y_{4.5}Co_2La_{1.5}$ powder as a function of particle size when atomized in nitrogen and argon. The insets are SEM back-scattered electron (SEM-BSE) images showing the microstructures of three powder particles of diameters ~16 μm, ~38 μm, and ~50 μm. The uniform and featureless phase contrast of the 16-μm-diameter powder particle indicates that it is fully amorphous. Crystallized phases are occasionally visible in the ~25-μm-diameter powder particle (see Fig. 6 for details), whereas substantial crystallization is readily observable in the 38-μm-diameter powder particle. The 50-μm-diameter powder is dominated by large crystallites.

Figure 2 shows typical XRD patterns obtained from the four size ranges of $Al_{86}Ni_6Y_{4.5}Co_2La_{1.5}$ powder. They are generally consistent with the SEM-BSE observations. Small Bragg peaks are noted for powder particles of <25 μm, but these particles are still essentially amorphous. Partial crystallization is clear in particles of 25–47 μm by XRD. When the particle size is >47 μm, Bragg peaks from crystalline phases dominate the XRD patterns, indicative of almost full crystallization. No intermediate phase was detected as the particle size increases.

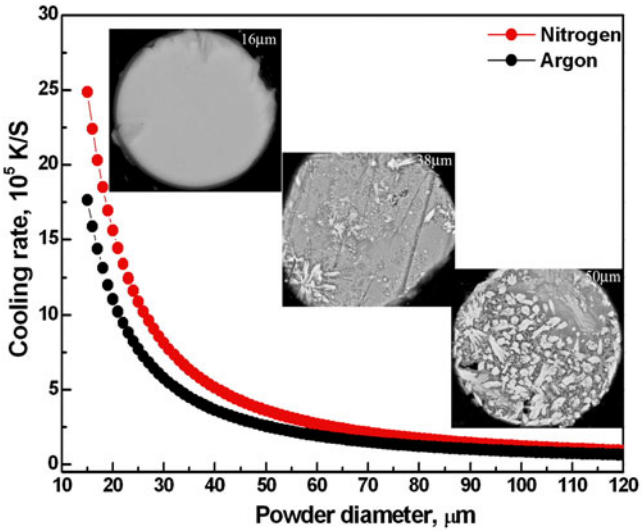


FIG. 1. Cooling rate variations with powder diameter of gas-atomized $Al_{86}Ni_6Y_{4.5}Co_2La_{1.5}$; nitrogen facilitates faster cooling than argon. SEM-BSE image insets show the microstructural evolution with powder diameter.

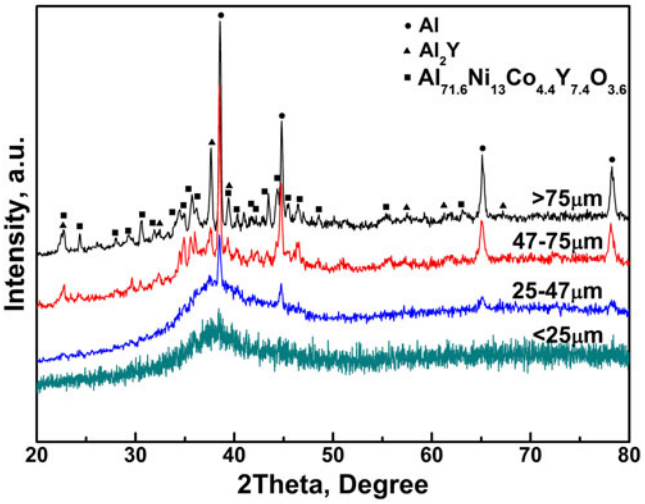


FIG. 2. XRD results for $Al_{86}Ni_6Y_{4.5}Co_2La_{1.5}$ powder of different sizes.

https://doi.org/10.1557/jmr.2011.13 Published online by Cambridge University Press

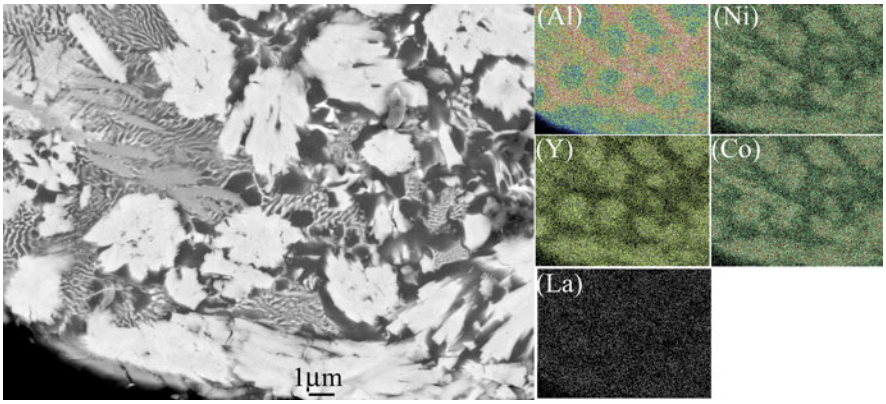


FIG. 3. SEM-BSE image of the microstructure of ~60-μm-diameter powder particle and corresponding elemental mapping of Al, Ni, Y, Co, and La. The BSE image reveals three major phase contrasts in the microstructure.

Consequently, characterization of the crystallized phases was focused on the large diameter powder particles.

B. Major crystalline phases by nitrogen atomization

Figure 3 presents the results of SEM elemental mapping obtained from the microstructure of a 60-μm-diameter particle. Three major phase regions are noted: (i) Al-enriched, (ii) (Al + Y)-enriched, and (iii) (Ni + Co + Y)-enriched. Figure 4(a) shows a TEM bright field (TEM-BF) image of the solidification microstructure of an FIB-prepared sample, where the three phase regions are denoted as P1 (Al-enriched), P2 [(Al + Y)-enriched], and P3 [(Ni + Co + Y)-enriched]. Detailed TEM characterization [Figs. 4(b) and 4(c)] identified that P1 is face-centered cubic (FCC) Al (a = 0.405 nm) and P2 is FCC-structured Al_2Y (a = 0.786 nm).

The (Ni + Co + Y)-enriched phase (P3) shows characteristics of an orthorhombic structure with a large lattice parameter in its c axis, but no information is available in the Joint Committee on Powder Diffraction Standards (JCPDS) database. It is likely a new phase. To determine its crystal structure, a series of selected-area-electron-diffraction (SAED) patterns were taken [Fig. 5(a)], which were reconstructed in reciprocal space in Fig. 5(b). This allows for the determination of the lattice parameters of the new phase as a = 1.28 nm, b = 0.39 nm, and c = 1.58 nm with an orthorhombic structure; similar phase identification work can also be found in other studies.[27,28] Based on these diffraction results, most space groups within the orthorhombic crystal system can be excluded for their specific requirements for characteristic diffractions. The possible space group for this phase is, therefore, to be either P222, or Pmmm, or Pmm2.[29] Its composition is close to the formula of $Al_{71.6}Ni_{13}Co_{4.4}$
$Y_{7.4}O_{3.6}$ as found by TEM–EDX analysis.

It should be noted that the orthorhombic phase was observed mainly in particles that have undergone substantial crystallization. They were not detected in the 25-μm-diameter particles that just show some early stages of crystallization. This suggests that the orthorhombic phase was formed in the late stage of solidification.

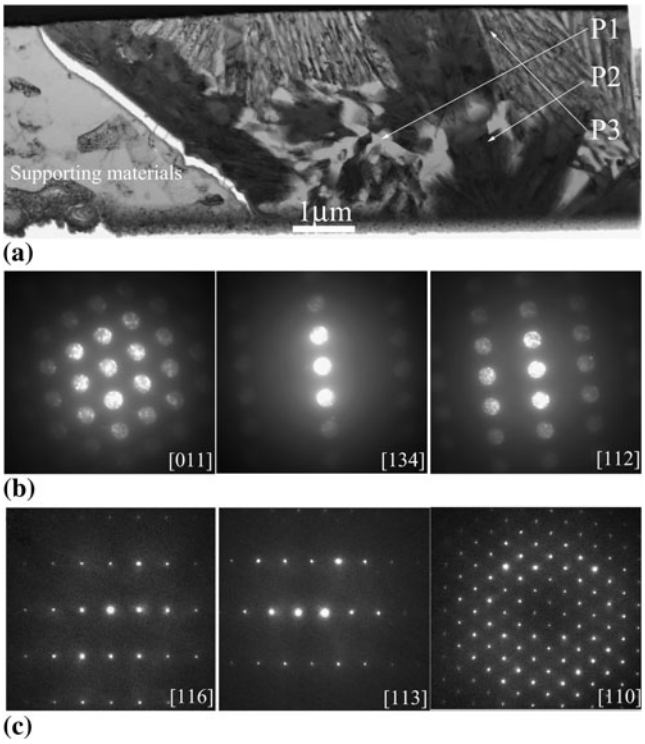


FIG. 4. Transmission electron microscopy (TEM) analysis of the microstructure of a 60-μm-diameter powder particle where the TEM sample was prepared by focused ion beam: (a) BF image of the solidification microstructure with the three major phases denoted as P1, P2, and P3; (b) SAED results for the phase of P1 (face-centered cubic (FCC)–structured Al phase); and (c) SAED results for the phase of P2 (FCC-structured Al_2Y phase).

C. Oxygen and nitrogen enriched Al_2Y phase

As indicated earlier, particles of 25-μm size are on the crystallization borderline. Smaller powder particles are

https://doi.org/10.1557/jmr.2011.13 Published online by Cambridge University Press

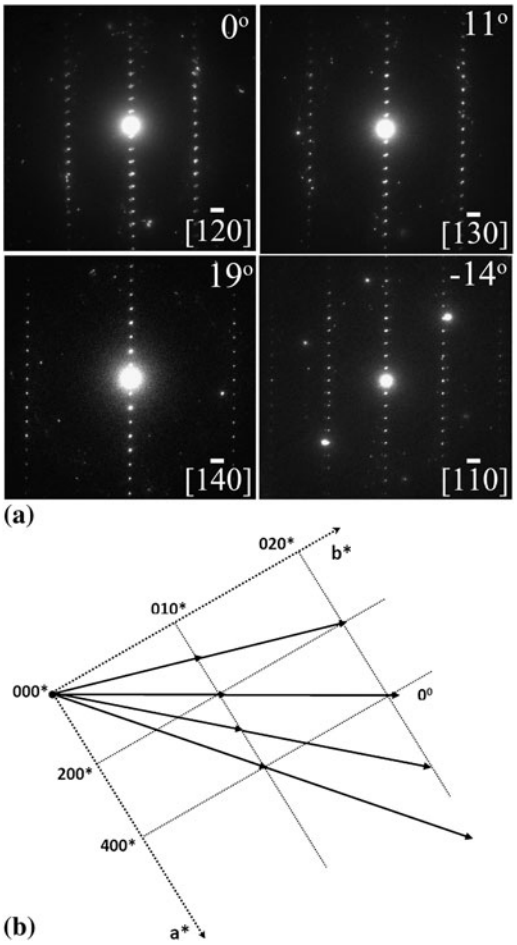


FIG. 5. TEM analysis of the phase of P3 shown in Fig. 4: (a) a series of SAED patterns obtained from the phase and (b) the reconstruction of the SAED patterns in reciprocal space.

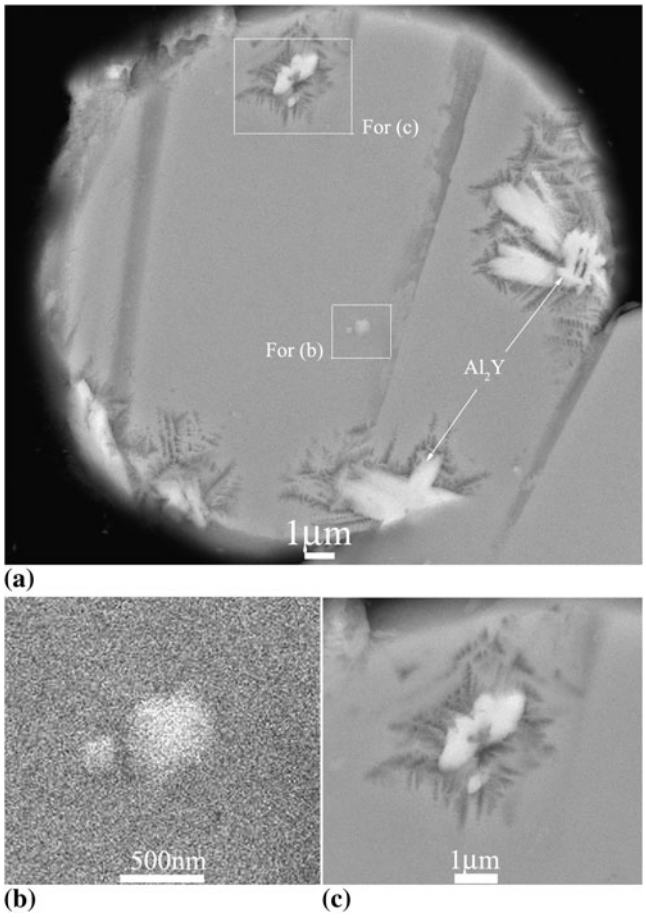


FIG. 6. SEM-BSE analysis of a 25-μm-diameter powder particle: (a) SEM image showing two crystallized phases (bright-contrast Al_2Y phase and dark-contrast Al phase); (b) and (c) are enlarged views of the marked areas in (a).

essentially amorphous, although crystallization is evident in larger particles. According to Eq. (1) and Fig. 1, the cooling rate for powder particles of this size during nitrogen atomization is $\sim 1.1 \times 10^6$ K/s. This value is higher than the general cooling rate range of gas atomization (10^2–10^5 K/s),[30] but it is still demonstrated to be achievable by literature.[25] In contrast, a recent analysis of the gas-atomized $Al_{86}Ni_6Y_{4.5}Co_2La_{1.5}$ powder by non-isothermal DSC reveals that the critical cooling rate required for the alloy to form an amorphous structure is only $\sim 1.0 \times 10^3$ K/s, which was determined using a method described in Ref. [31]. The detailed analysis is presented by Li et al. (unpublished data). An approximately three-order magnitude of difference thus exists with the critical cooling rate calculated by Eq. (1). In other words, the actual GFA of the alloy decreased significantly in a nitrogen-atomizing environment. Similar levels of inconsistencies have been reported for other amorphous alloy systems,[17,32] but the reasons remain unclear.

To understand the inconsistency, the microstructure of a ~25-μm-diameter powder particle was investigated in detail. As shown in Fig. 6(a), the particle shows two types of crystalline phase regions via SEM–BSE image: (Al + Y)-enriched and Al-enriched regions. Figures 6(b) and 6(c) show enlarged views of two selected areas from Fig. 6(a). Through TEM–SAED and TEM–EDX analysis, the matrix of this powder particle was amorphous [Fig. 7(a)], whereas the (Al + Y)-enriched phase was confirmed to be Al_2Y [Figs. 7(b) and 7(c)]; the other phase was crystalline Al [Figs. 7(d) and 7(e)]. Apart from the Bragg peaks that correspond to the FCC-Al, the XRD patterns of the powder with 25–47-μm diameter show an additional peak at ~37.5°, which matches with the Al_2Y phase (Fig. 2). Moreover, a considerable amount of oxygen (12.8 at.%) and nitrogen (5.6 at.%) was detected in the Al_2Y phase. The crystalline Al phase contained much less oxygen (~4.4 at.%) and a negligible amount of nitrogen. The corresponding TEM–EDX results are shown in Fig. 8(a). Additional evidence for nitrogen having been involved in the solidification of the alloy during nitrogen atomization was provided by XPS analysis and is shown in Figs. 8(b) and 8(c). Signals of N1s are detected at the binding energy of

https://doi.org/10.1557/jmr.2011.13 Published online by Cambridge University Press

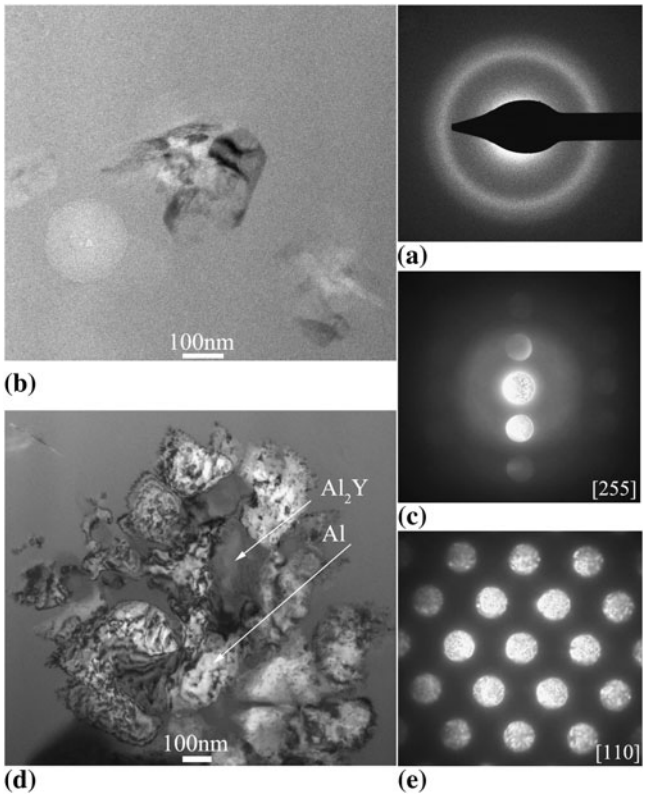


FIG. 7. TEM analysis of the 25-μm-diameter powder particle: (a) SAED for the amorphous matrix, (b) and (c) BF image and SAED results for the Al_2Y phase, (d) and (e) BF image and SAED results for the crystalline Al phase.

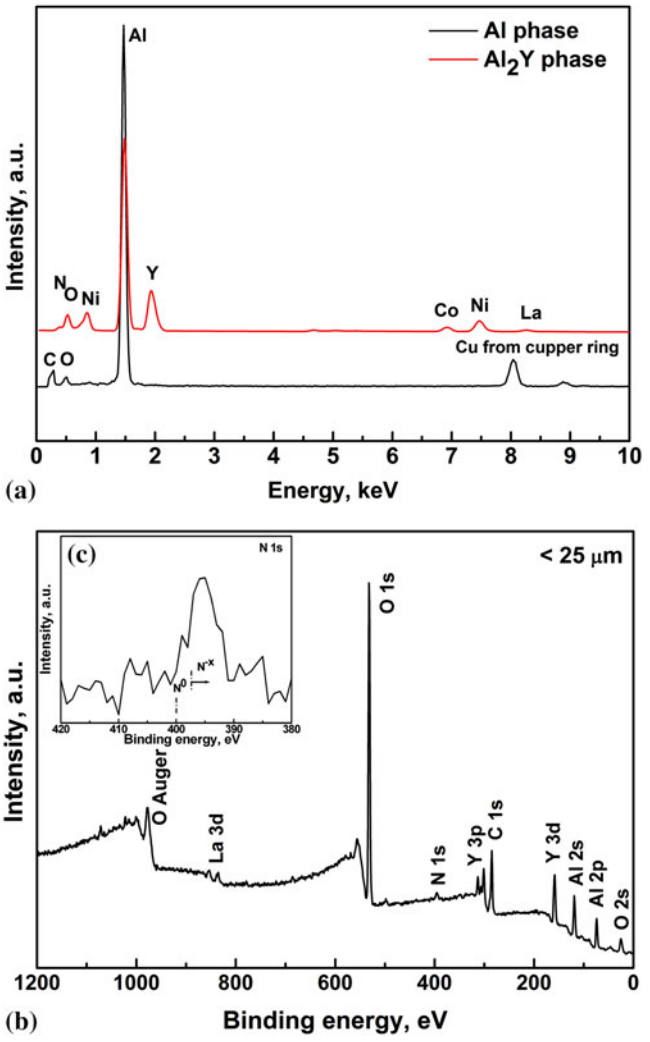


FIG. 8. (a) TEM–energy dispersive x-ray spectra for the crystalline Al phase and Al_2Y phase detected in ~25-μm-diameter powder particle, (b) XPS for a similar powder particle, and (c) a fine analysis of the state of N on the particle surface.

~397 eV [Fig. 8(b)]. More importantly, a further analysis of the N1s spectrum [Fig. 8(c)] indicates that the nitrogen detected exists in a state of substitutional N^{x-} [33,34] and it is not in the form of N_2 that is absorbed or attached onto the powder surface.

Unlike nitrogen, oxygen is a common impurity in many BMGs. It has been well documented that the presence of oxygen can greatly decrease the GFA of a glass-forming alloy.[11,12,35,36] In contrast, little information is available about the effect of nitrogen. The TEM–EDX and XPS analyses shown above suggest that both oxygen and nitrogen are involved in the precipitation of the Al_2Y phase. Regarding oxygen, it is difficult to avoid its impurity levels during gas atomization. With respect to nitrogen, although it facilitates faster cooling than argon in terms of the same liquid droplet size (Fig. 1), it is clearly not a desired medium for atomizing Y-containing aluminum amorphous alloys.

D. Sequence of solidification

A closer inspection of the microstructures of ~25-μm-diameter particles reveals that there exist free-standing single phase particles of Al_2Y in the microstructure [Fig. 6(b)], whereas the FCC-Al phase is always associated with the Al_2Y phase [Figs. 6(a) and 6(c)]. This indicates that Al_2Y can form independently during solidification and that it has likely solidified before the formation of the FCC-Al. The noticeably coarser particle sizes of the Al_2Y phase [Fig. 6(a)] are consistent with the inference. In other words, Al_2Y is the leading crystallization phase rather than the FCC-Al. And as a summary, the solidification sequence of $Al_{86}Ni_6Y_{4.5}Co_2La_{1.5}$ can be described as given below on the basis of the foregoing microstructural analysis:

$$\begin{aligned}\text{Liquid} &\rightarrow \text{Liquid}' + Al_2Y \rightarrow \text{Liquid}'' \\ &+ Al_2Y + Al \rightarrow Al_2Y + Al \\ &+ Al_{71.6}Ni_{13}Co_{4.4}Y_{7.4}O_{3.6} \quad .\end{aligned}$$

The fact that it is the Al_2Y phase rather than the Al phase that leads the crystallization process demonstrates a unique aspect of the novel $Al_{86}Ni_6Y_{4.5}Co_2La_{1.5}$ BMG.

https://doi.org/10.1557/jmr.2011.13 Published online by Cambridge University Press

For marginal glass-forming alloys like Al-based metallic glasses, curbing the growth of competing crystalline phase (s) holds the key to enhance the GFA, whereas nucleation control is more suited to good glass formers.[37] As the formation of Al_2Y requires more complex redistribution of the solute atoms compared with the formation of the FCC-Al, a higher kinetic barrier will be incurred to the growth of Al_2Y. This assists in understanding the observed excellent GFA of the alloy. The phenomenon distinguishes $Al_{86}Ni_6Y_{4.5}Co_2La_{1.5}$ from most other Al-based metallic glasses, which are generally believed to contain a large quantity of short-ranged and medium-ranged Al clusters responsible for the easy crystallization of the FCC-Al either during solidification[38] or after solidification.[39,40] A thermodynamic understanding of the driving force for the formation of the Al_2Y and FCC-Al and the interface energy for the Al_2Y/amorphous interface and the FCC-Al/amorphous interface is expected to shed light on the phase selection between Al_2Y and FCC-Al and the importance for the GFA of the alloy. Based on the current findings, tuning the relative concentration of the important constituent element, Y, in $Al_{86}Ni_6Y_{4.5}Co_2La_{1.5}$ could be a practical approach to further improve the GFA, as demonstrated on other glass-forming systems.[2,12,41,42]

IV. CONCLUSIONS

(1) An orthorhombic-structured phase has been identified in the partially or fully crystallized microstructure of $Al_{86}Ni_6Y_{4.5}Co_2La_{1.5}$. It has lattice parameters of a = 1.28 nm, b = 0.39 nm, and c = 1.58 nm, with an approximate composition of $Al_{71.6}Ni_{13}Co_{4.4}Y_{7.4}O_{3.6}$.

(2) Al_2Y, Al, and the orthorhombic $Al_{71.6}Ni_{13}Co_{4.4}Y_{7.4}O_{3.6}$ phase are the major phase constituents identified in the coarse powder particles of $Al_{86}Ni_6Y_{4.5}Co_2La_{1.5}$. Al_2Y is the leading crystalline phase during solidification, followed by the precipitation of the FCC-Al phase. The orthorhombic phase is formed in the final stage. Al_2Y rather than FCC-Al being the leading crystalline phase reveals an essential feature of this Al-based BMG.

(3) Apart from oxygen, nitrogen is also found to be closely associated with the formation of the leading crystalline phase Al_2Y in $Al_{86}Ni_6Y_{4.5}Co_2La_{1.5}$. It is proposed that nitrogen has enhanced the crystallization of Al_2Y during nitrogen atomization. Nitrogen is not recommended as a gas-atomizing medium for Al–Ni–Y-based metallic glass alloys.

ACKNOWLEDGMENTS

This work is supported by the Australian Research Council (ARC) and the National Key Basic Research Program of China (Grant No. 2007CB613906). Dr. M. Yan acknowledges the support of an ARC Postdoctoral Fellowship. We also acknowledge the technical, scientific, and financial assistance from the AMMRF.

REFERENCES

1. H.S. Chen and D. Turnbull: Formation, stability and structure of palladium-silicon based alloy glasses. *Acta Metall.* **17**, 1021 (1969).
2. Z.P. Lu, C.T. Liu, J.R. Thompson, and W.D. Porter: Structural amorphous steel. *Phys. Rev. Lett.* **92**, 245503 (2004).
3. V. Ponnambalam, S.J. Poon, and G.J. Shiflet: Fe-based bulk metallic glasses with diameter thickness larger than one centimeter. *J. Mater. Res.* **19**, 1320 (2004).
4. A. Inoue, W. Zhang, T. Zhang, and K. Kurosaka: High-strength Cu-based bulk glassy alloys in Cu-Zr-Ti and Cu-Hf-Ti ternary systems. *Acta Mater.* **49**, 2645 (2001).
5. W. Zhang, Q.S. Zhang, C.L. Qin, and A. Inoue: Formation and properties of new Cu-based bulk glassy alloys with critical diameters up to 1.5 cm. *J. Mater. Res.* **24**, 2935 (2009).
6. Y.C. Kim, W.T. Kim, and D.H. Kim: A development of Ti-based bulk metallic glass. *Mater. Sci. Eng. A* **375**, 127 (2004).
7. X.H. Lin and W.L. Johnson: Formation of Ti-Zr-Cu-Ni bulk metallic glasses. *J. Appl. Phys.* **78**, 6514 (1995).
8. H. Men and D.H. Kim: Fabrication of ternary Mg-Cu-Gd bulk metallic glass with high glass-forming ability under air atmosphere. *J. Mater. Res.* **18**, 1502 (2003).
9. H. Ma, L.L. Shi, J. Xu, Y. Li, and E. Ma: Discovering inch-diameter metallic glasses in three-dimensional composition space. *Appl. Phys. Lett.* **87**, 181915 (2005).
10. A. Peker and W.L. Johnson: A highly processable metallic-glass $Zr_{41.2}Ti_{13.8}Cu_{12.5}Ni_{10.0}Be_{22.5}$. *Appl. Phys. Lett.* **63**, 2342 (1993).
11. M. Yan, J. Zou, and J. Shen: Effect of over-doped yttrium on the microstructure, mechanical properties and thermal properties of a Zr-based metallic glass. *Acta Mater.* **54**, 3627 (2006).
12. M. Yan, J. Shen, T. Zhang, and J. Zou: Enhanced glass-forming ability of a Zr-based bulk metallic glass with yttrium doping. *J. Non-cryst. Solids*. **352**, 3109 (2006).
13. D.B. Miracle, T. Egami, K.M. Flores, and K.F. Kelton: Structural aspects of metallic glasses. *MRS Bull.* **32**, 629 (2007).
14. A.L. Greer and E. Ma: Bulk metallic glasses: At the cutting edge of metals research. *MRS Bull.* **32**, 611 (2007).
15. B.J. Yang, J.H. Yao, J. Zhang, H.W. Yang, J.Q. Wang, and E. Ma: Al-rich bulk metallic glasses with plasticity and ultrahigh specific strength. *Scr. Mater.* **61**, 423 (2009).
16. A. Inoue: Amorphous, nanoquasicrystalline and nanocrystalline alloys in Al-based systems. *Prog. Mater. Sci.* **43**, 365 (1998).
17. P. Dong, W.L. Hou, X.C. Chang, M.X. Quan, and J.Q. Wang: Amorphous and nanostructured Al(85)Ni(5)y(6)Co(2)Fe(2) powder prepared by nitrogen gas-atomization. *J. Alloy. Comp.* **436**, 118 (2007).
18. J.R. Hirth: Nucleation, undercooling and homogeneous structures in rapidly solidified powders. *Metall. Trans. A* **9A**, 401 (1978).
19. J.H. Perepezko and D.H. Rasmussen: Discussion of "Nucleation, undercooling and homogeneous structures in rapidly solidified powders". *Metall. Trans. A* **9A**, 1490 (1978).
20. S.A. Miller and R.J. Murphy: A gas-water atomization process for producing amorphous powders. *Scr. Metall.* **13**, 673 (1979).
21. G.Q. Xie, W. Zhang, D.V. Louzguine-Luzgin, H. Kimura, and A. Inoue: Fabrication of porous Zr-Cu-Al-Ni bulk metallic glass by spark plasma sintering process. *Scr. Mater.* **55**, 687 (2006).
22. M. Yan, P. Yu, K.B. Kim, J.K. Lee, G.B. Schaffer, and Ma Qian: The surface structure of gas-atomized metallic glass powders. *Scr. Mater.* **62**, 266 (2010).
23. Q.J. Zhai, Y.L. Gao, W.B. Guan, and K.D. Xu: Role of size and cooling rate in quenched droplet of Sn-Bi eutectic alloy. *Mater. Sci. Eng. A* **441**, 278 (2006).
24. E.S. Lee and S. Ahn: Solidification progress and heat-transfer analysis of gas-atomized alloy droplets during spray forming. *Acta Metall. Mater.* **42**, 3231 (1994).

https://doi.org/10.1557/jmr.2011.13 Published online by Cambridge University Press

25. M. Yang, Y.X. Dai, C.J. Song, and Q.J. Zhai: Microstructure evolution of grey cast iron powder by high pressure gas atomization. *J. Mater. Process. Tech.* **210**, 351 (2010).
26. D.J. Wang: Thermal stability and sintering behavior of TiCuZrNiSn metallic glass. Ph.D. Thesis, Harbin Institute of Technology, China, 2010.
27. J.A. Gard: Interpretation of electron-diffraction patterns, in *Electron Microscopy in Mineralogy*, edited by H.R. Wenk, P.E. Champness, J.M. Cowley, A.H. Heuer, G. Thomas and N.J. Tighe (Springer-Verlag, Berlin, 1976), pp. 52–67.
28. M. Yan, J. Zou, and J. Shen: New crystalline phases formed in a slowly-cooled Zr-based metallic glass. *J. Alloy. Comp.* **433**, 120 (2007).
29. T. Hahn (editor): *International Tables for Crystallography* (D. Reidel Publishing Company, Holland, 1983).
30. N.H. Pryds and A.S. Pedersen: Rapid solidification of martensitic stainless steel atomized droplets. *Metall. Mater. Trans. A* **33A**, 3755 (2002).
31. A. Inoue, T. Zhang, and T. Masumoto: Glass-forming ability of alloys. *J. Non-Cryst. Solids.* **156**, 473 (1993).
32. Y. Liu, Z.M. Liu, S. Guo, Y. Du, B.Y. Huang, J.S. Huang, S.Q. Chen, and F.X. Liu: Amorphous and nanocrystalline $Al_{82}Ni_{10}Y_8$ alloy powder prepared by gas atomization. *Intermetallics* **13**, 393 (2005).
33. J.F. Moulder, W.F. Stickle, P.E. Sobol, and K.D. Bomben, in *Handbook of X-ray Photoelectron Spectroscopy*, edited by J. Chastain (Perkin-Elmer Corporation, Minnesota, 1992).
34. R.G. Palgrave, D.J. Payne, and R.G. Egdell: Nitrogen diffusion in doped TiO_2 (110) single crystals: A combined XPS and SIMS study. *J. Mater. Chem.* **19**, 8418 (2009).
35. A. Gebert, J. Eckert, and L. Schultz: Effect of oxygen on phase formation and thermal stability of slowly cooled $Zr_{65}Al_{7.5}Cu_{7.5}Ni_{10}$ metallic glass. *Acta Mater.* **46**, 5475 (1998).
36. B.S. Murty, D.H. Ping, K. Hono, and A. Inoue: Influence of oxygen on the crystallization behavior of $Zr_{65}Cu_{27.5}Al_{7.5}$ and $Zr_{66.7}Cu_{33.3}$ metallic glasses. *Acta Mater.* **48**, 3985 (2000).
37. J.H. Perepezko: Nucleation-controlled reactions and metastable structures. *Prog. Mater. Sci.* **49**, 263 (2004).
38. H.W. Yang, P. Dong, J.Q. Wang, and Y. Li: Glass formability and structural stability of Al-based alloy systems. *Mater. Sci. Eng. A* **449–451**, 273 (2007).
39. F. Audebert, C. Mendive, and A. Vidal: Structure and mechanical behavior of Al-Fe-X and Al-Ni-X rapidly solidified alloys. *Mater. Sci. Eng. A* **375**, 1196 (2004).
40. J.H. Perepezko, R.J. Hebert, and W.S. Tong: Amorphization and nanostructure synthesis in Al alloys. *Intermetallics* **10**, 1079 (2002).
41. J. Chen, Y. Zhang, J.P. He, K.F. Yao, B.C. Wei, and G.L. Chen: Metallographic analysis of Cu-Zr-Al bulk amorphous alloys with yttrium addition. *Scr. Mater.* **54**, 1351 (2006).
42. Y. Zhang, J. Chen, G.L. Chen, and X.J. Liu: Glass formation mechanism of minor yttrium addition in CuZrAl alloys. *Appl. Phys. Lett.* **89**, 131904 (2006).

https://doi.org/10.1557/jmr.2011.13 Published online by Cambridge University Press